25th ABCM International Congress of Mechanical Engineering
October 20-25, 2019, Uberlândia, MG, Brazil

COB-2019-2069
EXTERNAL DYNAMIC BEHAVIOR OF AN INDUSTRIAL ROBOTIC SYSTEM

Wesley R. Oliveira[1]
Aline da C. Matheus[2]
Wilson José de Sá Marques[3]
Luís G. Trabasso[4]
Emília Villani[5]
Guilherme B. Rodamillans[6]
ITA - Aeronautics Institute of Technology
Division of Mechanical Engineering (IEM) – Manufacturing Competence Center (CCM)
wesleyro@ita.br[1]
aline.matheus@ccm-ita.org.br[2]
wilsonsamarques@ccm-ita.org.br[3]
gonzaga@ita.br[4]
evillani@ita.br[5]
guilhermebr@ccm-ita.org.br[6]

Abstract: *This paper presents an alternative approach to the identification of industrial robotic system dynamics, which is viewed as a closed-loop Position IN/Position OUT system. The emphasis is on the external dynamics of a conventional 7 degrees-of-freedom (7DoF) serial manipulator with its real-time positional controller. The identified model represents how an external client application interacts with its internal control-loop. The identification experiment is presented and the results concerning the external observed dynamics are discussed. This approach is intended to support integration, validation of simulations and accurate online path-planning algorithms, as it shall be expected in the context of robotic flight simulators and sensor-integrated industrial robotic systems.*

Keywords: industrial robot, dynamic modeling, robot identification, real-time robotic systems.

1. INTRODUCTION

Since its advent in the industrial environment in the early 1960s, dynamic modeling and parametric identification of industrial robots have attracted much attention from researchers and industrials due to their importance to model-based control, integration, validation of simulation results and accurate path planning algorithms (Wu, Wang & You, 2010). An extensive literature has been produced on that and, still nowadays, the problem of finding the physical dynamic/kinematic parameters of the manipulator[1] in different situations comprises a full research line (Atkeson, An & Hollerbach, 1986; Gautier, Khalil & Restrepo, 1994; Yasuho, Omaki, Nampo & Mayeda, 1997; Swevers, Verdonck & De Schutter, 2007; Gautier, Janot & Vandanjon, 2008; Ding, Wu, Yao, Yang, 2015).

Strictly speaking, the vast majority of the related literature focus on the classical identification problem of the well-known multivariable coupled nonlinear dynamic model of the industrial manipulator physics (Wernholt, 2004). This model is represented in Eq. (1) in its closed analytical form (Craig, 2012; Yasuho, Omaki, Nampo & Mayeda, 1997).

$$\mathbf{M}\left(\bar{\theta}\right)\ddot{\bar{\theta}} + \mathbf{C}\left(\bar{\theta},\dot{\bar{\theta}}\right)\dot{\bar{\theta}} + \bar{\gamma}\left(\bar{\theta}\right) = \bar{\tau}(t) \tag{1}$$

where $\bar{\theta}$, $\dot{\bar{\theta}}$, $\ddot{\bar{\theta}}$ are the *nx1* instantaneous joint angles, velocities and accelerations vectors, respectively; $\mathbf{M}\left(\bar{\theta}\right)$ is the so-called *nxn* inertial-mass matrix; $\mathbf{C}\left(\bar{\theta},\dot{\bar{\theta}}\right)$ is the *nxn* aggregated centrifugal and Coriolis matrix; $\bar{\gamma}\left(\bar{\theta}\right)$ is an *nx1* vector of gravitational-related terms; and $\bar{\tau}(t)$ is the *nx1* vector of the applied joint torques over the time. From Eq. (1), it is clear that the manipulator is nonlinear at the operating point (besides further nonlinearities such as friction, backlash

[1] Hereinafter the term manipulator is used to refer to serial robot arm as defined in ISO 8373 (2012), "i.e. mechanism consisting of a series of segments/links jointed or sliding relative to one another". Though also interesting, the identification of the dynamics of fully parallel mechanisms, usually a more complex problem, is disregarded in this work. Guegan, Khalil & Lemoine (2003) and Wu, Wang & You (2010) can be read on this subject.

and others not explicitly considered in the formulation above). Furthermore, it is a coupled multivariable system, since the motion of one joint cause reactions on the previous joints. Additionally, industrial robots pose a challenging identification problem because they are inherently unstable systems in open-loop and the experimental data must be collected while the robot controller is operating in closed-loop (Wernholt, 2004).

Therefore, the standard robot identification approach is complex, though still suitable for the intents of systems' stability analyses and model-based control (Atkeson, An & Hollerbach, 1986; Swevers, Verdonck & De Schutter, 2007). Nonetheless, such an approach is based on the assumption that the robot controller itself has an open-architecture so that the control laws could be further adjusted or, at least, the actual control strategies used along the closed-loop identification are known. While this can be understood as a premise for the robot developers, it is rarely the situation for the final users of commercial-off-the-shelf industrial robots, which seldom present an open-architecture controller.

Considering the aforementioned aspects, this work deals with the subject of robotic system dynamics identification with a different perspective. The identification emphasis put herein is on the input/output measurable positional signals from the industrial robotic system, as depicted in Fig. 1.

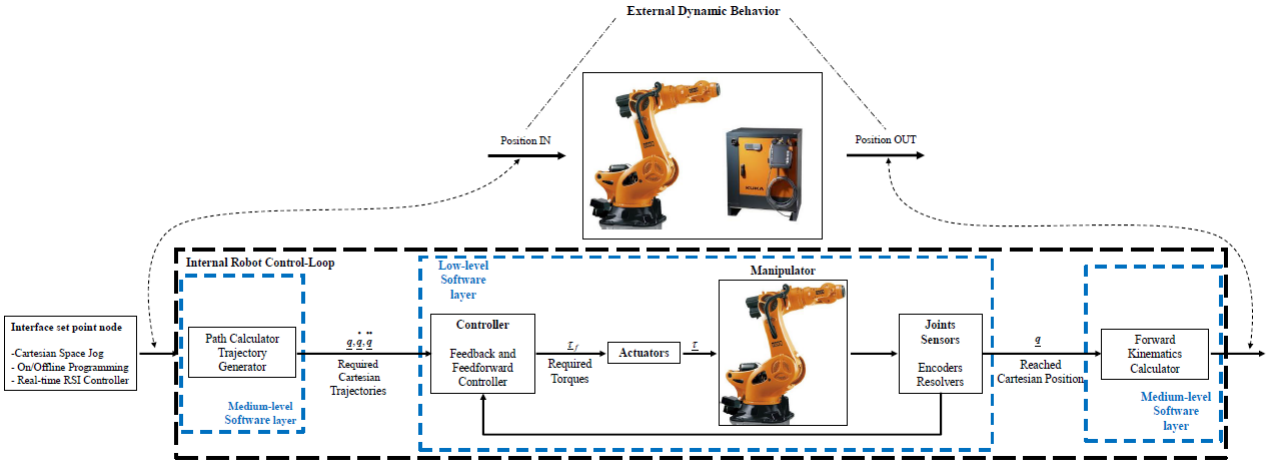

Figure 1. Industrial robotic system viewed as a positional closed-loop system.

As shown in Fig. 1, the term "Robotic System" is used throughout this work to refer to the closed-loop positional system comprising the Position In/Position Out relationship. This embodies the manipulator physics under the controller actions, representing the external behavior perceived by the end-user application with which the robotic system interacts. The main assumption is that the industrial robotic system can supply a real-time (online and deterministic) interface to command its internal control-loop with an adequate time latency – at least one tenth of the lower mechanical time-constant (Ogata, 1995). This would be lower than 50 ms for a heavy-payload robot with a time-constant of 500 ms for the joint dynamics (Teufel et. al., 2007). This applies to some industrial robots like the KUKA® KR-500 with the Robot Sensor Interface (RSI) controller, used by Teufel et. al. (2007) and Marx et. al. (2008). The robot analyzed in this work is the KUKA® KR-Titan, a 1-ton payload robot.

The identification process for such external dynamic behavior of the robotic system, as employed in this work, follows a standard approach consisting of: model selection; experiment design; data acquisition; signal processing; parameter estimation; and model validation (Swevers, Verdonck & De Schutter, 2007). Although the approach emphasized herein could be seen as simplified black-box identification, this work discusses some significant aspects such as decoupling limits, frequency behavior and additional dynamic characteristics of the robot. Regardless of not being useful for torque estimation and therefore model-based control, this approach is intended to support integration and validation of simulations, as it is necessary in the context of industrial digital simulation or robotic flight simulators (Teufel et. al., 2007; and Marx et. al., 2008).

2. MATERIALS AND METHODS

Figure 2 illustrates the 'Quad-M' framework for systems identification, as applied in this work (Jategaonkar, 2006). The *Maneuver* design is the first step. It should excite the system dynamics in the frequency range of interest. The next *'M'* in the sequence is due to the *Measurements*, which is related to how to properly collect and process data during the experiments with the real plant. Thirdly, the selection of the *Method* is performed, which is intrinsically related to the chosen optimization algorithm. Finally, the *Model* structure (parametric or non-parametric) selection and estimation of its related parameters are performed. The last step is the validation of the identified model.

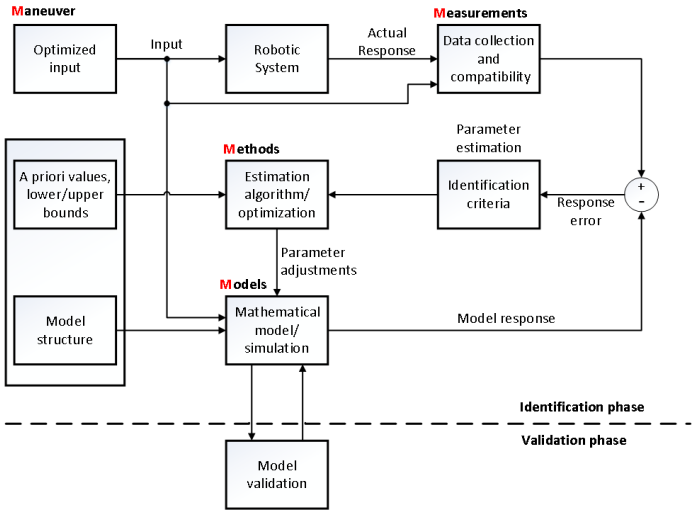

Figure 2. Quad-M Approach (Jategaonkar, 2006).

In this work, a time-domain black-box parametric identification approach is used, since the IN/OUT data from the closed-loop system is available from the KUKA® RSI controller with a 12 ms heartbeat, although a prior model structure is assumed as unknown (Isermann & Münchhof, 2011). Considering previous approaches (Teufel et. al., 2007; Marx et. al., 2008), the Cartesian-space architecture depicted in Fig. 3 is assumed and the identification is carried out for a KUKA® KR-Titan industrial manipulator (Fig 4). Figure 3 shows that when using the robotic system (manipulator + RSI controller) there may be some additional path calculator blocks for the Cartesian-space approach. Besides that, as previously demonstrated by Teufel et. al. (2007), the system always presents a transport-delay ($e^{-\Delta Ts}$) and a discrete moving average filter on the input. It is assumed a decoupling among the 7 DoF of the robotic system (the rail and the X, Y, Z , A, B and C for the Cartesian-space pose, with A, B, C representing the ZYX orientation Euler-Angles), so that the multivariable approach is reduced to seven independent single-input-single-output (SISO) channels corresponding to each DoF of the robot. This hypothesis is verified in the item 3.2.1 of this work.

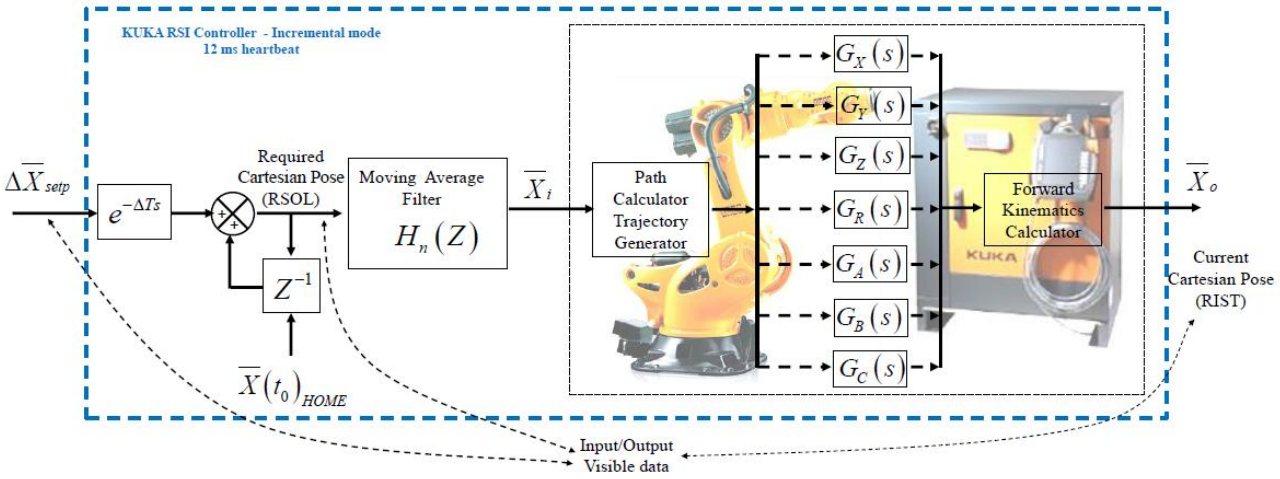

Figure 3. Block diagram of the Cartesian-space closed-loop of the KR-Titan.

2.1 *Maneuver design – excitation signals*

Figure 5 presents the identification signal designed for one of the channels (X-channel): a time-varying amplitude chirp-signal (Wernholt, 2004), which was designed to scan a frequency-band up to 5.2 Hz. This chirp signal is given by Eq.(2) and its parameters are optimized to excite the robot without taking it out from its actuation limit, what could enforce some nonlinearities disregarded in the above assumed structure. In total, experiments were performed with four different maximum excitation frequencies. The chirp-signals with bandwidth of 0.10, 1.04 and 5.20 Hz were used for identification while the signal within the intermediary range of 2.08 Hz was used for model validation.

Figure 4. KUKA® KR-Titan with a rail unit used in the experiments.

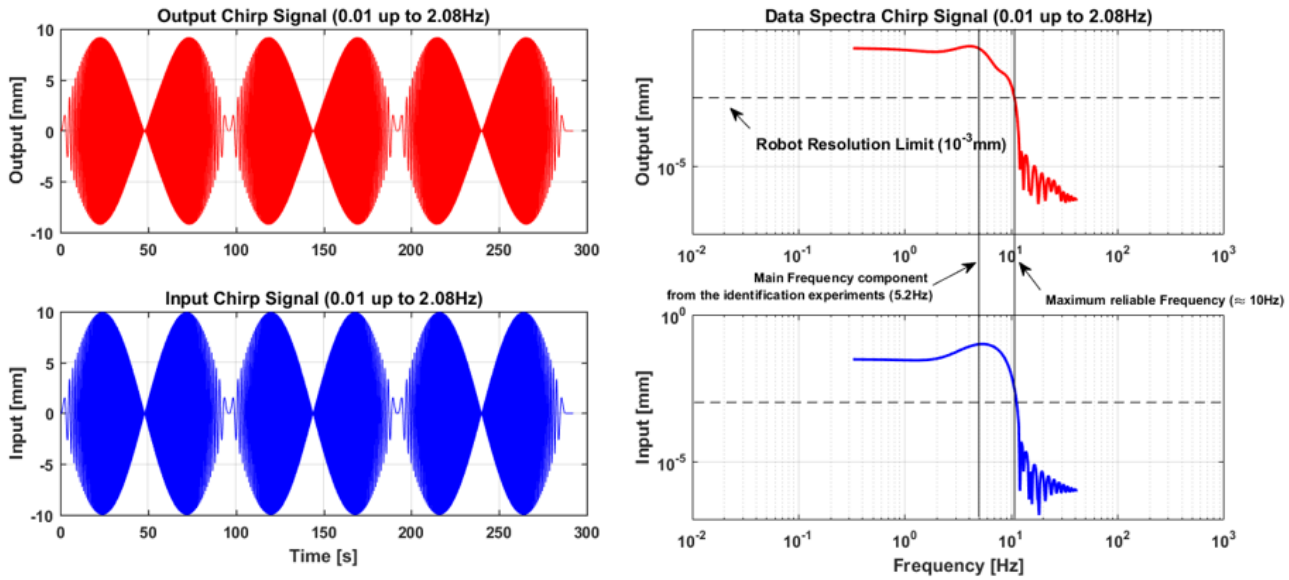

(a) (b)

Figure 5. Excitation (IN) and output (OUT) signals (a) and the signal spectra (b) used along the Cartesian-space identification experiment for channel X (in mm).

$$u_0(t) = A(t)\sin\left(2\pi f_1 t + \frac{\pi}{T_0}(f_2 - f_1)t^2 + \varphi\right), \quad 0 \le t \le T_0, \tag{2}$$

where $A(t)$ is the time-varying amplitude, with a triangular profile optimized to avoid driving the robot to a speed or acceleration limit according to the increasing of the frequency; f_1 is the lowest frequency (0.01 Hz) going through the frequency range, inversely to the slope of the amplitude modulation, up to f_2, the highest designed frequency component; φ is the phase (in *rad*); t is the time variable (in *s*), T_0 is the fundamental time interval (in *s*) considered for the periodicity of the resultant modulated chirp-signal (blue nodes in Fig. 5). Four different signals were used in the experiments, optimized to allow the evaluation of the robot behavior within the designed frequency spectra of 0.10 Hz up to 5.20 Hz. However, since the modulated amplitude introduces an additional time-varying behavior in the signal (meaning it is not a strictly stationary periodic signal), the actual excited frequency range may reach some higher values in some situations. For instance, in Fig. 5, for the nominal 5.20 Hz chirp-signal of the X-channel, the actual relevant spectrum (components with amplitude higher than the robot minimum resolution) reached values close to 10 Hz.

2.2 *Measurements*

Four experiments were run for each DoF in each frequency range. In order to explore the whole operational robot dynamic range, specific maximum amplitudes were selected in each case according to Table 1

Table 1. Maximum nominal amplitudes used along the identification experiment.

Frequency / Channel	0.01Hz ~ 0.1 Hz	0.01Hz ~ 1.04 Hz	0.01 Hz ~ 2.08 Hz	0.01 Hz ~ 5.2 Hz
Translation (X, Y, Z) (mm)	600	50	10	2
Rail (mm)	600	10	2	0.5
Rotation (A, B) (°)	35	2	0.5	0.1
Rotation C (°)	35	2	1	0.1

The input signals are position commands (in relation to the tool center point (TCP) coordinate frame) to be transmitted to the robot through a LabView®/Client application using an Ethernet/UDP protocol. Data with the current Cartesian pose (output of the robot) have also been obtained from the KUKA® RSI controller. The sampling time is the controller heartbeat of 12 ms (~84 Hz). In the experiments, the robot always started from the same home position of the robot targeted application, where the X-axis of the robot's TCP is aligned with X-axis of the robot's base and rail. The data was collected from the robotic system with an absolute error of 0.01 mm (translational) and 0.001° (rotational).

2.3 *Model structure*

The Linear Continuous Time-Invariant (LTI) transfer function model was chosen for the inner black-box transfer functions that are supposed to model the external Cartesian behavior of each DoF between the RSOLL (Input) and RIST (output) points depicted in Fig. 3. It encompasses the moving average block, the path calculator and the forward kinematics blocks, and the inner closed-loop behavior of the joints. The general structure for this kind of parametric model is given in Eq. (3) with b_i and a_i representing the numerator and denominator coefficients, respectively.

$$G(s) = \frac{C(s)}{U(s)} = \frac{b_0 s^m + b_1 s^m + ... + b_{m-1} s + b_m}{a_0 s^n + a_1 s^{n-1} + ... + a_{n-1} s + a_n} \qquad \mathbf{n > m} \tag{3}$$

2.4 *Method – optimization and validation*

For transfer function models, the parameters to be estimated are its poles and zeros. At this point, the System Identification Toolbox™ from Matlab® 2018b was used. The system order is sought to be kept as low as possible while achieving a goodness of fit greater than 90%, considering the Normalized Root Mean Square Error (NRMSE) (given in Table 2). A Gauss-Newton nonlinear least squares algorithm was used as the optimization method. Also, in order to guarantee the physical meaning of the model, the causality principle must be respect (Oppenheim, 1997), which translates into the numerator order being at least one order lower than the denominator. As previously mentioned, the set of IN/OUT signals with bandwidth of 0.1, 1.04 and 5.2 Hz were used for the identification of each DoF, yielding to 7 models to be estimated.

The quality of the identified models was validated by three statistical measures in relation to the set of IN/OUT validation signals (intermediary range of 2.08 Hz), namely: the coefficient of determination R^2, the Normalize Root Mean Square Error (NRMSE) and the Akaike's Final Prediction Error (FPE), whose formulations are summarized in Table 2. Note that the NRMSE was used instead of the more conventional RMSE, because comparisons are made among the validation responses of different models, gathered from different data sets with different amplitudes, so it was necessary to use a normalized quantity. The FPE measure gives an indication of the fidelity of the estimated model, taking into consideration the model complexity upon the examination of the number of parameters in the model.

Table 2. Summary of the main characteristics of the statistical measures.

Metric	Formula	Interval	Worst Fit	Best Fit
R^2	$1 - \frac{\sum_i (y_i - f_i)^2}{\sum_i (y_i - \bar{y})^2}$	0 ~ 1	0	1
NRMSE	$1 - \sqrt{\frac{\sum_i (y_i - f_i)^2}{\sum_i (y_i - \bar{y})^2}}$	-∞ ~ 1	-∞	1
FPE	$\det\left(\frac{1}{N}\sum_1^N e(t,\hat{\theta}_N)(e(t,\hat{\theta}_N))^T\right)\left(\frac{1+\frac{d}{N}}{1-\frac{d}{N}}\right)$	0 ~ 1	1	0

According to Table 2, for the measures R^2 and NRMSE, y_i represents the real value and f_i is the predicted value at the instant t_i, $\bar{y}$ is the mean. For the FPE measure, N is the number of values in the estimation data set, $e(t)$ is a $n \times 1$ vector of prediction errors, θ_N is the vector of estimated parameters and d is the number of estimated parameters.

3. RESULTS AND DISCUSSIONS

3.1 Identified models

The results for the identification experiment are described in this section, beginning with the presentation in Table 3 of the identified linear transfer function models for each of the robot's *DoF*.

Table 3. Identified models for each DoF of the robot.

Channel	Transfer Function
X	$\frac{6.803\times10^4 s^2 + 5.917\times10^5 s + 1.247\times10^8}{s^4 + 1040s^3 + 9.076\times10^4 s^2 + 4.693\times10^6 s + 1.287\times10^8}$
Y	$\frac{60.68s^2 + 5488s + 1.657\times10^4}{s^3 + 227.1s^2 + 5978s + 1.657\times10^4}$
Z	$\frac{24.08s + 1362}{s^2 + 65s + 1362}$
R	$\frac{5.491s^2 + 1273s + 8453}{s^3 + 48.41s^2 + 1529s + 8453}$
A	$\frac{25.65s + 762.2}{s^2 + 48.72s + 762.1}$
B	$\frac{-6.254s^2 + 6863s + 1.032\times10^4}{s^3 + 205.1s^2 + 7179s + 1.032\times10^4}$
C	$\frac{-1906s + 1.053\times10^5}{s^2 + 1846s + 1.049\times10^5}$

According to Table 3, with the exception of the model for the X-channel, all the inner models for the channels converged to a model of order lower or equal to 3. This is the representation of the robot closed-loop behavior that, though of restricted interpretation due to the black-box assumption, resembles to a jerk-controlled positional system, which is a common parameterization for path-planning controlled robotic systems (Craig, 2012). However, this is just a reflection, since the presented results with the current assumptions do not allow further physical interpretations. On the other hand, the X-channel presented an unforeseen behavior yielding to a more complex order model and this specific aspect will be discussed in detail below.

Another worth mentioning point is in regard to the transfer functions for channels B and C, which presented negative coefficients in their numerator. Firstly, this fact is not viewed as a surprising one since it has not been made any kind of restriction on the values the coefficients could assume along the identification. Thus, the negative coefficients could in fact be potentially obtained. Phisically speaking, these negative coefficients in the numerator of the transfer function indicates the presence of a zero in the right half of the complex plane, as confirmed by the root locus and the step response plots in Fig. 6. This type of system is referred in the literature as a nonminimum-phase system, and its main characteristic is to present a step response that moves downwards before of properly following the reference (Ogata, 1995; Franklin et al, 1994). All that can be affirmed on this topic, considering the collected experimental data, is that the system seems to present a pretty similar behavior to those depicted in Fig. 6 to the theoretical step-response behaviors. Besides that, it is worth to stress this is a closed-loop behavior. This aspect should be further investigated in future works, with some additional external measurement systems that also tracks the accelerations performed by the robot arm during the experiments. Notwithstanding, the resulting model for the robotic system presented satisfactory validation performance for all the DoF, as evinced by the results in Table 4.

3.2 Models' time response - validation

Figure 7 shows the time response of the models, with their related 97% confidence boundaries and the expected output measured from the real robot system, for one period of excitation of the 2.08 Hz chirp-signal. All the three

models of the rotational channels had a very good fit, with a range of motion of about 0.5 degrees in both directions.

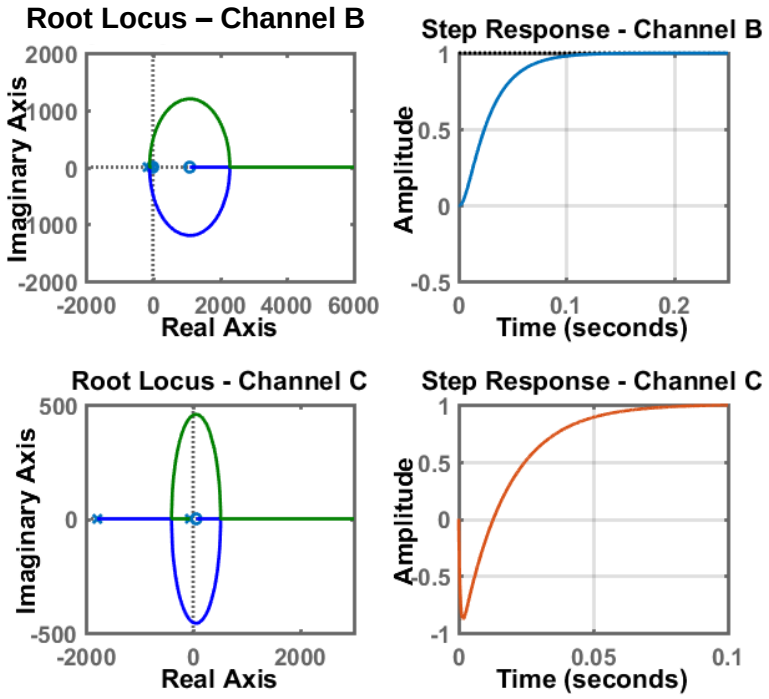

(a) (b)

Figure 6 . Root locus (a) and Step Response (b) plots for channels B and C.

Table 4. Statistical measures for the identified models.

Channel / Metric	X	Y	Z	R	A	B	C
R^2	0.998	0.996	1.000	1.000	1.000	1.000	1.000
NRMSE	0.958	0.935	0.984	0.966	0.984	0.986	0.997
FPE	0.0014	0.065	0.001	0.003	0.000	0.000	0.000

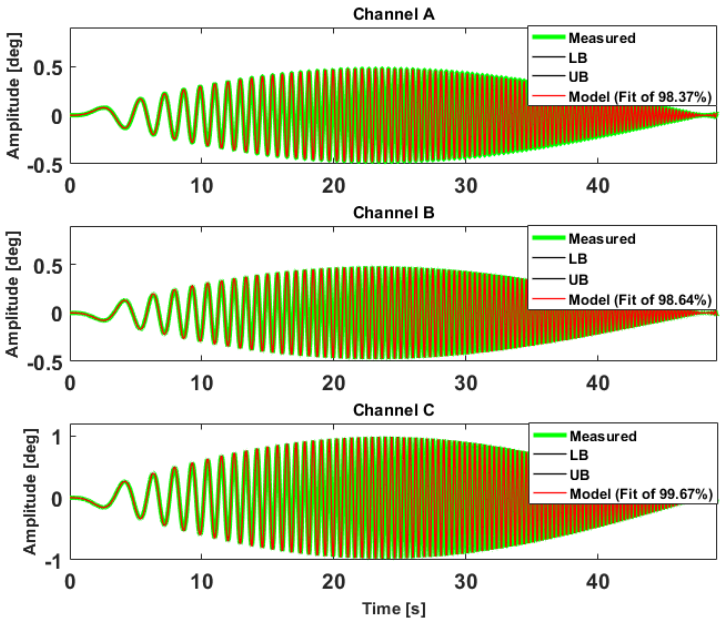

Figure 7. Validation time-responses to the 2.08 Hz chirp-signal for the rotational channels (A, B and C), where LB and UP stands for the 97% confidence level lower and upper bounds, respectively.

Figure 8 illustrates the same information for the translational channels. In this case, the model for the channel Y was the one with the worst fit (yet good, with a NRMSE of 93%). The range of motion of the robot during the experiments was about +/-10 mm for X, Y and Z channels, while of +/-2 mm for the Rail (channel R).

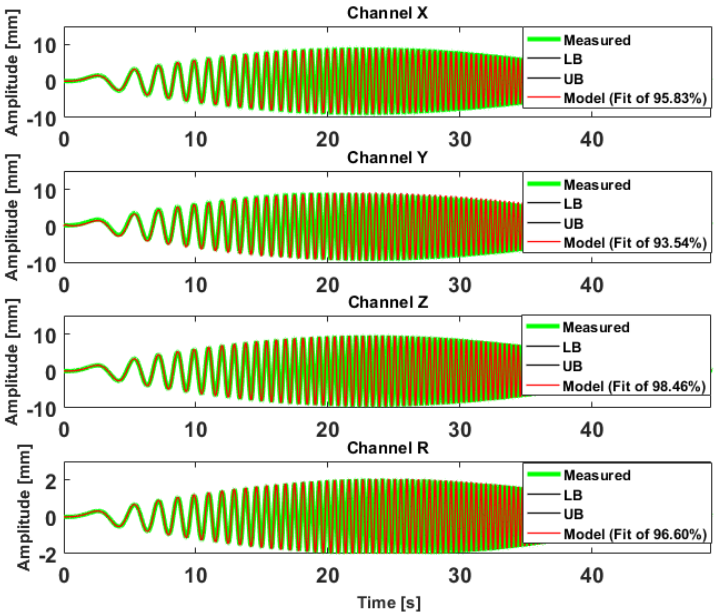

Figure 8. Validation time-responses to the 2.08Hz chirp-signal for the translational channels (X, Y, Z, R), where LB and UP stands for the 97% confidence level lower and upper bounds, respectively.

3.2.1 Verification of the decoupling hypothesis

In order to verify the hypothesis of decoupling among the Caretsian DoF. of the robotic system, in this section it is proposed an analysis that considers the root of the maximum value of the magnitude-squared coherence function (Kay, 1988) between each possible input/output paired signals of Cartesian DoF.. The magnitude-squared coherence is dimensionless function defined in the frequency domain that indicates a causality relation between two random signals (Ljung & Glad, 1994). Equation (4) presents the mathematical formulation for the metric used herein:

$$\gamma_{\max} = \max_{f} \sqrt{\frac{\left|P_{xy}(f)\right|^2}{P_{xx}(f)P_{yy}(f)}} \tag{4}$$

where $P_{xx}(f)$ and $P_{yy}(f)$ is the power spectral density for the random signals x (which generically represents a system's input) and y (which generically represents a system's output), respectively, and $P_{xy}(f)$ is the cross power spectral density of x and y. If the coherence value (γ_{max}) is close to one, it means the two signals are well related.

Besides of that, it is added a criteria to evaluate the plausibility of the possible causality relation, which is the dimensionless magnitude ratio (RIst/RSol) for each combination of inputs/output pairs. Since it is is a dimensionless number, a normalization process is necessary when analising the relation between a translational DoF and a rotational DoF. The ratio of the robot resolution, 0.00001°/0.001mm, is applied for that.

Figure 9 depicts a mapping of the coherence values, frequency range of the excitation input signal and the magnitude ration between the input and the output for every possible combination of inputs/output pairs for the Cartesian degrees of freedom of the robotic system. The coherence value is plotted on the x-axis, the frequency in which the experiments were ran goes on the y-axis and the magnitude ratio between the signal response (RIst) and the signal input (RSol) is the z-axis.

In Fig. 9, it is noticed that the coherence values between the degrees of freedom can be higher (> 0.70) in any frequency range of the excitation signals used along the identification experiment. However, they are clearly more pronounced for the higher frequency ranges (squared markers corresponding to the frequency range up to 5.20 Hz), where one can notice a huge concentration of the points in the map. It is worth to stress that all the auto-relations (those presenting the same DoF. for the input and the output, as, for instance, RSol_X with RIst_X) are higher than 0.70 (actually, close to 1), which is in accordance to the expected closed-loop tracking behavior of the robot. Notwithstanding, from the perspective of the magnitude ratio, taking as a threshold criteria for relevant causality those relations that are higher than 0.15, it is noticed that the causality relations that are significant are basically the auto-

relations cases. The only exceptions are the relations RIst_X/RSol_Z, RIst_Z/RSol_R, RIst_X/RSol_R, RIst_Z/RSol_X, which are strictly regarded to the frequency range of up to 5.20Hz, evincing a clear limit of the decoupling hypothesis used throughout this paper. Summarizing, this means that the model identified and presented in this work is valid for an excitation signal within the range of up to 2.08 Hz.

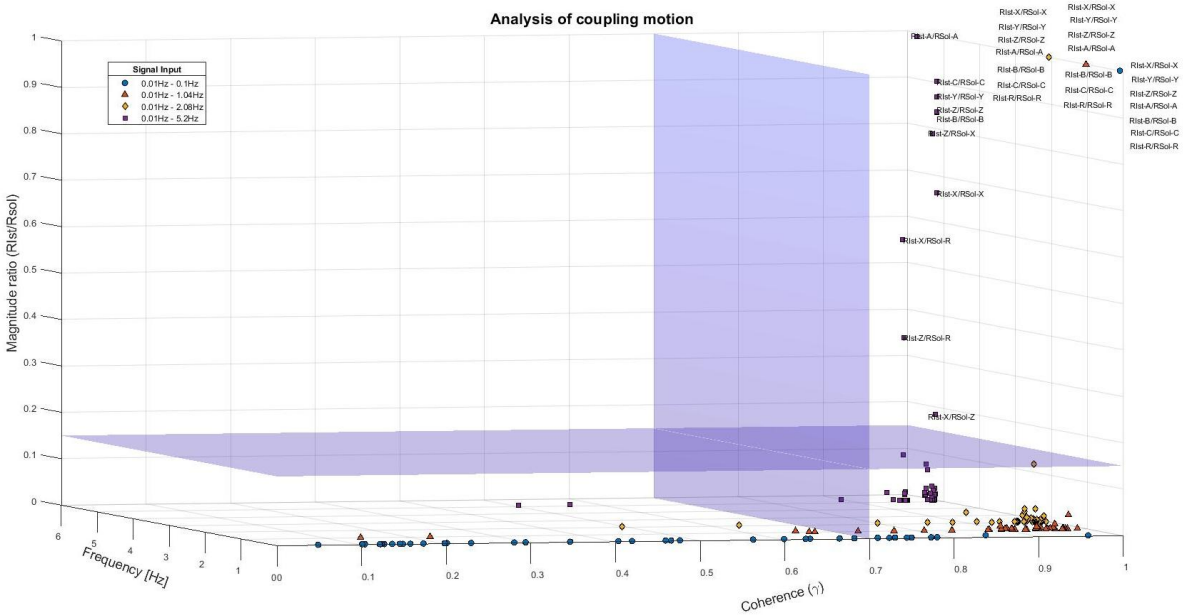

Figure 9. Mapping of the coupling motion for the combination of inputs/output pairs of Cartesian DoF..

3.3 Models' frequency response

Figure 10 gives the frequency behavior by means of the bode plots of (a) the estimated empirical transfer function models (ETFE) and b) the identified transfer function models for each of the rotational channels. The ETFE is computed as the ratio of the output Fourier transform to the input Fourier transform. It can be noticed that channels B and C presented a dominant damped second order behavior, with the magnitude curve decaying at a -20 dB/dec rate (Ogata, 1995). Channel A seems to present a resultant dominant first order decaying for both the magnitude and the phase curves, resembling to a more rigid DoF. In these graphics, relevant frequencies are up to 62,8 rad/s.

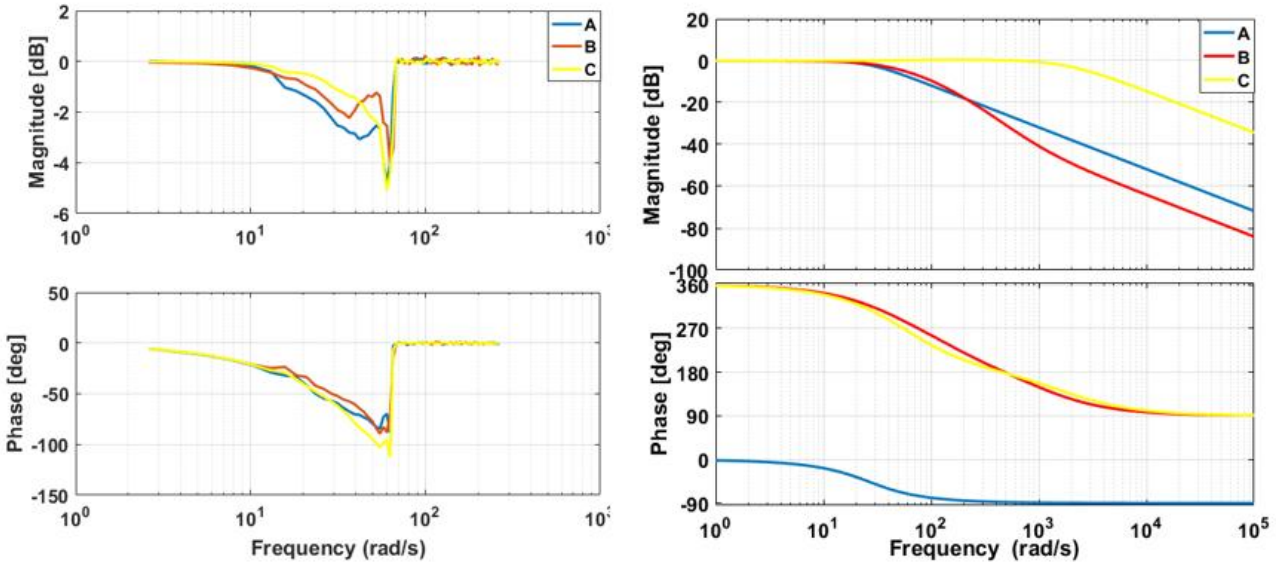

Figure 10. Bode plots for the rotational channels. (a) ETFE and (b) Transfer function.

Figure 11 presents the bode plots for each of the translational channels. In these graphics, relevant frequencies are

up to 62,8 rad/s. Here, the most intriguing behavior was observed in the X-channel, which presented also the most complex transfer function (Table 3). For this particular case, it can be seen a response characteristic to a notch (band-stop) filter around the frequency of 6.0 Hz. From first experimental analyses, this showed to be a possible close-loop characteristic compensation from a mechanical resonant mode of the robotic arm and the rail. Such behavior has been noticed when the experiment was performed around the chosen home position, where the TCP's X-axis, the Base's X-axis and the rail are all aligned together. Unusually, this characteristic response changes if the experiment departs from different home positions. Although the current results and assumptions do not allow to precisely identifying the frequency of the arm's excitation mode, they suggest it may occur around 6.0 Hz. As it would normally be expected a high displacement from a mechanical resonance of the robot arm, it has been reasonably compensated by the controller.

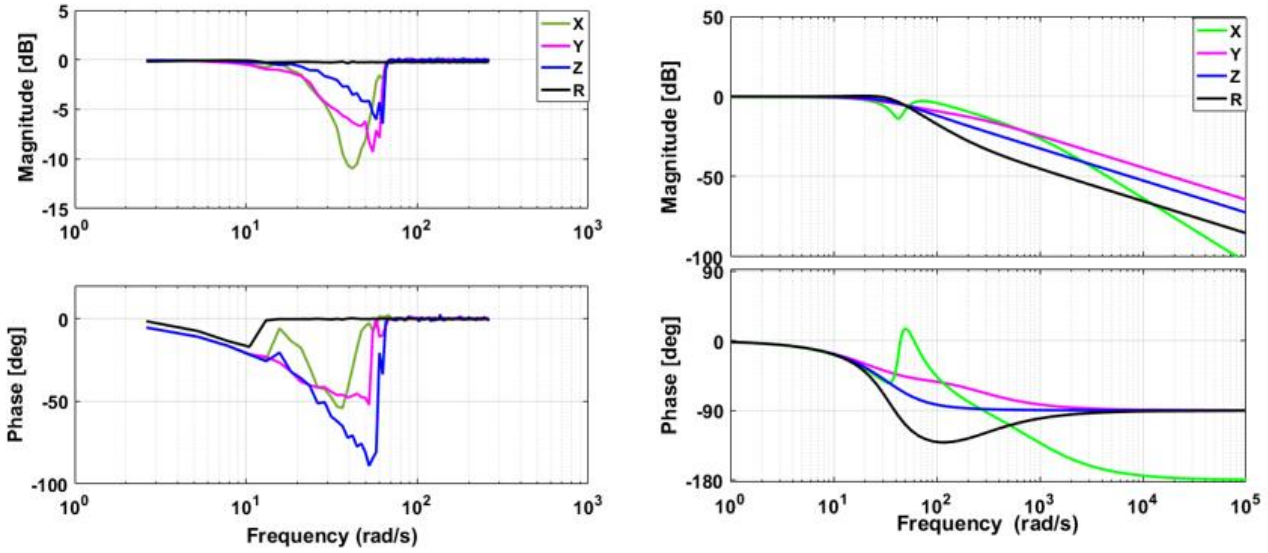

Figure 11. Bode plots for the translational channels. (a) ETFE and (b) Transfer function.

4. CONCLUSIONS

The primary goal of this work was fulfilled as it analyzed and described in detail a possible approach for the identification of industrial robots. It contributed to the understanding of the closed-loop dynamics of the commercial-off-the-shelf heavy-payload industrial manipulator KUKA® KR-Titan. As an additional innovative contribution, the model presented included also the linear unit (rail) dynamics, a feature that has not been noticed in similar works. In relation to the validation of the presented results, the final robot model showed an agreement greater than 93% for all the DoF, being presented as a reliable tool for future developments. From the identification experiment, a closed-loop notch filter behavior has been detected for one of the Cartesian channels (X), what might be a unique characteristic of this robotic arm. Future developments of this work will include the identification upon data acquired with an inertial measurement device (accelerometers and rate gyros) and the use of MIMO identification techniques to obtain models that contemplate situations where the decoupling hypothesis assessed in *3.2.1* does not apply. Additionally, a state observer for velocities and accelerations streaming shall be implemented in a future release of the obtained model.

5. REFERENCES

Atkeson C. G.; An, C. H.; Hollerbach, J. M., 1986, "Estimation of inertial parameters of manipulator loads and links". In: International Journal of Robotics Research", Vol. 5, Issue 3, pp. 101-119. SAGE, 1986.

Craig, J. J., 2012, "Robótica / John J. Craig". Original English Title: *Introduction to robotics: mechanics and control*., 3. ed.. São Paulo, Pearson Education do Brasil, 2012.

Ding, L.; Wu, H.; Yao, Y. & Yang, Y., 2015, "Dynamic Model Identification for 6-DOF Industrial Robots". In: Journal of Robotics, Vol. 2015, ID 471478, pages 9. Hindawi Publishing Corporation, 2015. DOI: 10.1155/2015/471478.

Franklin, Gene F., et al. Feedback control of dynamic systems. Vol. 3. Reading, MA: Addison-Wesley, 1994.

Gautier, M.; Janot, A.; Vandanjon, P. O., 2008, "DIDIM: a new method for the dynamic identification of robots from

only torque data". In: Proceedings of the IEEE International conference on robotics and automation (ICRA 2008), pp. 2122-2127. Pasadena-USA, 2008. DOI: 10.1109/ROBOT.2008.4543520.

Gautier, M.; Khalil, W., Restrepo, P. P., 1995, "Identification of the dynamic parameters of a closed loop robot". In: Proceedings of IEEE International Conference on Robotics and Automation (ICRA 1995), pp. 3045-3050. Nagoya-Japan, 1995. DOI: 10.1109/ROBOT.1995.525717.

Guegan, S.; Khalil, W. & Lemoine, P. "Identification of the Dynamic Parameters of the Orthoglide". In: Proceedings of IEEE – International Conference on Robotics and Automation 3:3272-3277, vol. 3, October-2003. DOI: 10.1109/ROBOT.2003.1242095.

Isermann, R. & Münchhof, M., 2011, "Identification of Dynamic Systems: An Introduction with Applications". Springer, Berlin, 2011. DOI: 10.1007/978-3-540-78879-9.

Jategaonkar, R. V., Flight Vehicle System Identification: A Time Domain Methodology, Vol. 216, Progress in Aeronautics and Astronautics, AIAA, 2006, p. 12 - 13.

Kay, Steven M. Modern Spectral Estimation. Englewood Cliffs, NJ: Prentice-Hall, 1988.

Ljung, L. & Glad, T., 1994, "Modelling of Dynamic Systems". Prenice-Hall, 1994. ISBN: 0-13-597097-0.

Marx, M.; Conconi, M.; Tändl, M. & Kecskeméthy, A. "Optimized kinematical positioning and guidance of a serial robot for motion simulation", In: (IAK 2008) Proc. of the Conference on Interdisciplinary Applications of Kinematics. Lima-Peru, 9-11 January, 2008.

MathWorks-Matlab®, (2018). Optimization Toolbox™: Constrained Nonlinear Optimization Algorithms (R2017b). Available online: https://www.mathworks.com/help/optim/ug/constrained-nonlinear-optimization-algorithms.html. Access: July 3rd, 2018.

Swevers, J.; Verdonck, W.; De Schutter, J., 2007, "Dynamic model identification for industrial robots". In: IEEE Control Systems Magazine, Vol. 27, Issue 5, pp. 58–71. IEEE, 2007. DOI: 10.1109/MCS.2007.904659.

Ogata, K., 1995, "Dicrete-Time Control Systems", 2nd Edition, Chap. 3, pp. 92. Prentice-Hall, New Jersey, 1995.

Oppenheim, A. V.; Willsky, A. S. Signals *& Systems.* 2nd Edition, Chap. X, p. X. Upper Saddle River, N.J.: Pearson, 1997.

Teufel, H.J., Nusseck, H.G., Beykirch, K.A., Butler, J.S., Kerger, M., and Bülthoff, H.H., 2007, "MPI Motion Simulator: Development and Analysis of a Novel Motion Simulator". AIAA Modeling and Simulation Technologies Conference and Exhibit, Vol. 1, AIAA, Hilton Head, South Carolina, 2007, p. 1 - 11.

Wernholt, E., 2004, "On Multivariable and Nonlinear Identification of Industrial Robots". PhD Thesis No. 1131 (Doctoral in Electrical Engineering – Control Systems), DEE, Linköping University. Linköping/Sweden, 2004.

Wu, J.; Wang, J. & You, Z., 2010, "An overview of dynamic parameter identification of robots". In: Journal of Robotics and Computer-Integrated Manufacturing (JRCIM), Vol. 26, pp. 414-419. Elsevier, 2010.

Wu, W.; Zhu, S.; Wang, X. & Liu, H., 2012, "Closed-loop Dynamic Parameter Identification of Robot Manipulators Using Modified Fourier Series". In: International Journal of Advanced Robotic Systems, Vol. 9, Issue 29, pages 9. INTECH, 2012. DOI: 10.5772/45818.

Yasuho, T.; Imaki, Y.; Nampo, T. & Mayeda, H., 1997, "Identification and Model Based Control of a 6 DOF. Industrial Manipulator". In: Proceedings of 5h IFAC Symposium on Robot Control (SYROCO '97), Vol. 30, Issue 20, pp. 111-117. Elsevier, 1997. DOI: 10.1016/S1474-6670(17)44252-2.

6. RESPONSIBILITY NOTICE

The author(s) is (are) the only responsible for the printed material included in this paper.